PROCEEDINGS OF SPIE

SPIEDigitalLibrary.org/conference-proceedings-of-spie

Brillouin-like effects in rare-earth-doped bi-directional optical fiber amplifiers

Andrei Fotiadi, Dmitry Korobko, Ivan Chapalo, Patrice Megret, Igor Zolotovskii

Andrei Fotiadi, Dmitry Korobko, Ivan Chapalo, Patrice Megret, Igor Zolotovskii, "Brillouin-like effects in rare-earth-doped bi-directional optical fiber amplifiers," Proc. SPIE 12569, Nonlinear Optics and Applications XIII, 125690I (5 June 2023); doi: 10.1117/12.2665902

SPIE.

Event: SPIE Optics + Optoelectronics, 2023, Prague, Czech Republic

Brillouin-like effects in rare-earth-doped bi-directional optical fiber amplifiers

Andrei Fotiadi[a,b], Dmitry Korobko[c], Ivan Chapalo[b], Patrice Megret[b], Igor Zolotovskii[c]
[a]Optoelectronics and Measurement Techniques Unit, University of Oulu, 90570 Oulu, Finland
[b]University of Mons, Boulevard Dolez 31, 7000 Mons, Belgium.
[c]Ulyanovsk State University, 42 Leo Tolstoy Street, Ulyanovsk, 432970, Russia.

ABSTRACT

Brillouin amplification, the most prominent effect implemented with Brillouin dynamical gratings (BDG), enables exponential narrowband gain that is Stokes-shifted by some value in the GHz range. In this process, the interaction of the counterpropagating pump and Stokes waves through a BDG they produce causes an increase of the Stokes-shifted wave amplitude and decrease of the pump wave amplitude during their propagation through the fiber. Here, we report on a similar effect that could be implemented in rare-earth-doped fibers with the population inversion dynamical gratings. The effect is the most pronounced in a bidirectional rare-earth-doped optical fiber amplifier. Two monochromatic optical signal waves are introduced into the fiber from opposite ends and experience amplification (if the fiber is pumped) or attenuation (if the fiber is unpumped) as they propagate through the fiber. The signal waves are coherent on a sub-kHz level and slightly detuned. In terms commonly accepted in stimulated Brillouin scattering these counterpropagating signal waves correspond to what is referred to as "pump" and "Stokes" waves. However, in contrast to the Brillouin process, their interference inside the rare-earth-doped fiber creates not acoustic, but the population inversion dynamical gain grating. Then interaction between the signal waves and created population inversion dynamical gratings cause a strong power transfer from one signal wave to another.

Keywords: Population inversion gratings; rare-earth doped fibers; stimulated Brillouin scattering

1. INTRODUCTION

In contrast to the stationary Fiber Bragg Gratings (FBG), the dynamical gratings (DG) can be implemented only temporarily in an optical fiber. The light-induced dynamic gratings are inscribed through the interaction between the optical medium and an interference pattern formed by a number of coherent light waves[1]. A physical mechanism responsible for dynamic grating inscription strongly depends on the media properties. Acoustic waves enhanced by a stimulated Brillouin scattering (SBS) in optical fibers create a refractive index grating known as Brillouin dynamic grating (BDG) that has recently emerged as a flexible tool for optical processing, microwave photonics and distributed sensing [2-7]. The population inversion dynamical gratings (PIDG) inscribed by counterpropagating optical waves in rare-earth-doped fibers are responsible for rather slow or even stationary dynamical effects[8, 9]. In standing-wave lasers, spatial hole burning induces a static grating of the population inversion, enabling multimode operation with several independent lasing modes [10]. In open-cavity fiber lasers, the slowly-moving dynamical population inversion gratings inscribed in an active medium by intracavity radiation have a reverse effect on the inscribing waves via feedback they provide leading to so called “mode-pulse” laser operation different from mode-locked and Q-switched laser regimes [11, 12]. Among other PIDG applications are adaptive interferometry[13, 14] and nonlinear filtering enabling narrowband operation of semiconductor and fiber laser configurations[15-18].

Here, we present a theoretical formalism to describe the amplification of two monochromatic waves counter-propagating in a rare-earth-doped optical fiber amplifier. Interaction of the waves through a dynamical population inversion grating inscribed in the active fiber by the waves during their amplification results in a strong power transfer from one wave to another providing a preferable amplification of one wave at the expense of another. In this sense, the effect is similar to stimulated Brillouin scattering and is expected to be observed with both pumped and unpumped rare-earth-doped fibers possessing a finite polarizability difference between the excited and ground states.

Brillouin amplification, the most prominent effect implemented with BDG, enables exponential narrowband gain that is Stokes-shifted by some value in the GHz range[19, 20]. In this process, the interaction of the counterpropagating pump and Stokes waves through a BDG they produce causes an increase of the Stokes-shifted wave amplitude and decrease of

Nonlinear Optics and Applications XIII, edited by Mario Bertolotti, Anatoly V. Zayats, Alexei M. Zheltikov, Proc. of SPIE Vol. 12569, 125690I · © 2023
SPIE · 0277-786X · doi: 10.1117/12.2665902

the pump wave amplitude during their propagation through the fiber. Here, we report on a similar effect[21] that could be implemented in rare-earth-doped fibers with the PIDG. The propagation of the monochromatic wave through the active fiber could provide the counterpropagating wave with an additional gain shifted in frequency by some value in the kHz range. The effect is the most pronounced in a bidirectional rare-earth-doped optical fiber amplifier as it is employed for the amplification of two counter-propagating monochromatic waves. An interaction of the counterpropagating waves through a dynamical population inversion grating inscribed by them during amplification could cause a strong power transfer from one wave to another. Like Brillouin amplification, the predicted effect exhibits a strong resonance dependence on the frequency difference $\Delta\omega = \omega^+ - \omega^-$, where $\omega^{\pm}$ denotes the frequencies of two monochromatic waves and the dynamical wave equations are similar to the SBS equations[22-25]. At each point in the fiber the most effective power transfer is achieved at the frequency difference $\Delta\omega$ matching the local grating relaxation time τ_G that is determined by the doping rare-earth-ion lifetime T and decreases with an increase of operating powers. In contrast to SBS, the power transfer in the rare-earth-doped fibers can occur either to the wave with higher (anti-Stokes) or lower (Stokes) frequency. Anti-Stokes wave amplification dominates in pumped fibers, while amplification of the Stokes wave could occur in fibers without pumping. In this paper, we give a clear physical insight into the Brillouin-like amplification in rare-earth doped optical fibers and present important details of the fiber model. In particular, the equations reproducing inscription of the population inversion gratings in the fiber by counterpropagating monochromatic optical signals and the dynamics of the reverse effect the inscribed gratings produce on the amplification process are derived and presented in terms of standard fiber specifications.

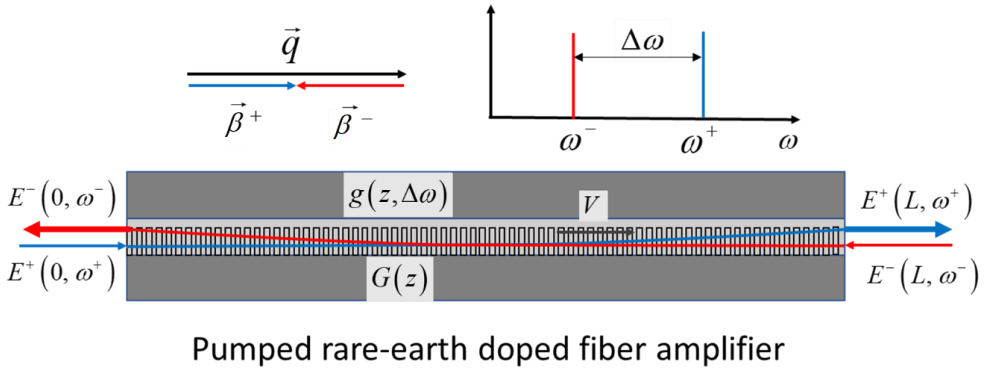

Figure 1. Amplification of counter-propagating waves in a rare-earth doped optical fiber.

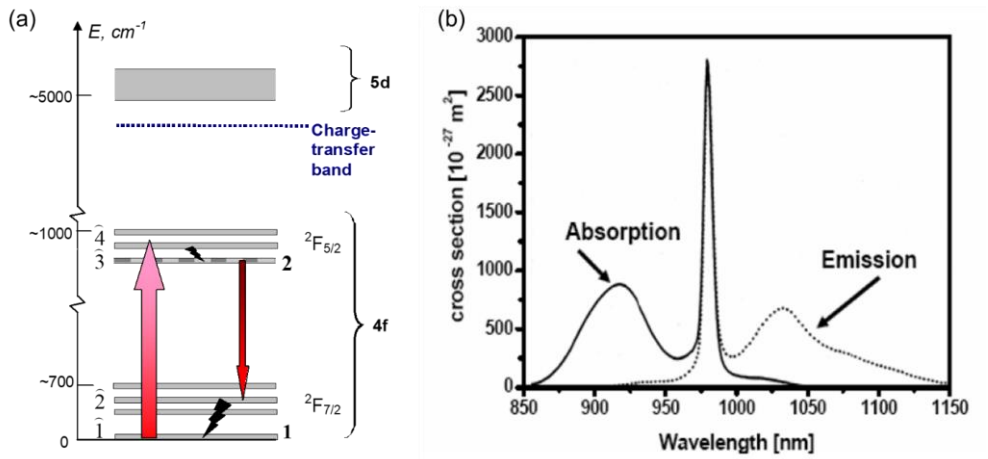

Figure 2. The atomic manifold level system (a) and emission and absorption cross section of ytterbium in silica host (b). 1, 2 and $\hat{1}, \hat{2}, \hat{3}, \hat{4}$ indicate the levels for two- and four- level laser models, respectively.

2. MATHEMATICAL MODEL

Let us consider a single-mode rare-earth-doped optical fiber shown in Fig.1. The fiber could be pumped from an external laser diode that creates the population inversion inside the fiber length providing an amplification to the optical signal waves propagating through the fiber. Without a loss of generality, we can assume in this paper that the fiber under consideration is an ytterbium-doped silica optical fiber. Silica glass, the most common material for manufacturing fibers, is a good host for Yb-ions[26]. The spectroscopy of the Yb-ion shown in Fig. 2(a) is simple compared to other rare-earth ions. For amplification in the optical spectrum range, only two-level manifolds are important: the ground-state manifold ($^2F_{7/2}$) and the excited-state manifold ($^2F_{5/2}$). Although they consist of four and three sublevels, respectively, the transitions between sublevels are smoothed due to strong homogeneous and inhomogeneous broadening. Yb-doped fibers are able to produce optical gain over a very broad wavelength range spanning from 975 to 1200 nm with a range of possible pump wavelengths from 860 nm to 1150 nm (Fig.2(b)). A number of pronounced laser effects governed by the population inversion mechanism have been observed in single-mode Yb-doped optical fibers under resonant diode pumping at 975 nm. Importantly, similar to other rare-earth-doped fibers the Yb-doped fibers are subjected to electronic refractive index change (RIC) effect that is the side effect of the population inversion mechanism[27]. Commonly, the two-level population laser model[28] is enough to provide an accurate interpretation to these effects as confirmed by multiple experimental observations. Here, we use the two-level population laser model to explore the Brillouin-like amplification in rare-earth-doped fibers and to demonstrate its spectral and dynamical properties.

In our consideration, we assume that the single-mode Yb-doped fiber is pumped at $\lambda_p \sim 975nm$. A couple of monochromatic optical signals at around $\lambda_s \sim 1060nm$ is introduced into the fiber from opposite ends as shown in Fig.1. and optical amplification in the fiber is available in both directions. Mathematically, we consider amplification of two monochromatic optical signals $E^{\pm}\exp\left[i\left(\omega^{\pm}t \mp \beta^{\pm}z\right)\right]$ at frequencies $\omega^{\pm}$ and with propagation constants $\beta^{\pm}$ propagating through the fiber in positive (+) and negative (-) directions, respectively. An external pumping (one- or two-directional) creates both the population density of Yb-ions in the excited state $N_2(z)$ and corresponding optical gain factor $G(z)$ smoothly distributed over the fiber. Due to the optical gain $G(z)$ the amplitudes $E^{\pm}$ increase as the optical signals propagate through the fiber.

On the other hand, the superposition of the amplified counter-propagating optical fields inside the fiber forms an interference pattern $I(t,x) \sim E^{+}E^{-*}\exp\left[i\left(\Delta\omega t - qz\right)\right]$ covering the whole fiber length, where the frequency difference is $\Delta\omega \equiv \omega^{+} - \omega^{-}$, the wavenumber is $q = \beta^{+} + \beta^{-} \approx 2\tilde{\omega}n/c$ and $\tilde{\omega} \equiv \left(\omega^{+} + \omega^{-}\right)/2$. The interference pattern $I(t,z)$ produces a spatial longitudinal modulation of the population density $N_2(z)$ in the fiber core $\delta N_2(t,z) \sim I(t,z)$ resulting in a similar modulation of the optical gain $\delta G(t,z) \sim I(t,z)$. Due to the electronic RIC effect mentioned above, the modulation of the optical gain $\delta G(t,z)$ is followed by the identical modulation of the fiber core refractive index $\delta n(t,z) \sim I(t,z)$. This bundle of quantities combined as $\Gamma = \left(\delta G + ik^0\delta n\right)\exp\left[i\left(\Delta\omega t - qz\right)\right]$ is referred to as the population inversion dynamical grating (PIDG). Here, the first and second terms are known as the amplitude (gain) and phase dynamical gratings, respectively. From the two-level model of the RIC effect in rare-earth-doped fibers[27] the grating amplitudes are:

$$\begin{aligned} \delta G &= \left(\sigma_{21}^{(s)} + \sigma_{12}^{(s)}\right)\rho_S(0)\delta N_2 \equiv \mathrm{Re}\, g \\ k^0\delta n &= \frac{4\pi^2 F_L^{\,2}}{\lambda_S n_0}\Delta p_d \delta N_2 \equiv \mathrm{Im}\, g \end{aligned} \qquad (1)$$

where $F_L = \left(n_0^{\,2} + 2\right)/3$ is the Lorentz factor; n_0 is the unperturbed refractive index, $\sigma_{21}^{(s)}$ and $\sigma_{12}^{(s)}$, are the emission and absorption cross-sections at optical signal wavelengths, $\rho_S(r)$ is the normalized radial distribution of the signal power; $k^0 = 2\pi/\lambda_S$ is the signal wave number in vacuum; $\Delta p_d = p_2 - p_1$, p_1 and p_2 are the polarizabilities of the Yb-ions in the ground and excited states, respectively. From Eqs.1, the ratio between the phase and gain grating amplitudes is fixed, since it is determined only by the operation wavelength λ_S and the polarizability difference Δp_d and does not depend on the operating powers:

$$\kappa \equiv \frac{\mathrm{Im}\, g(t,z)}{\mathrm{Re}\, g(t,z)} = \frac{\left(2\pi F_L\right)^2}{\lambda_S \left[n_0 \left(\sigma_{21}^{(s)} + \sigma_{12}^{(s)} \right) \rho_S(0) \right]} \Delta p_d \qquad (2)$$

It is a specific feature of the dynamical gratings inscribed through the population inversion mechanism. The polarizability difference Δp_d measured for Yb-doped fibers gives $\kappa = 2.7$ at $\lambda_S \sim 1060\ nm$ [27].

When the optical signal waves propagate through the fiber amplifier their amplitudes are changed due to optical gain $G(z)$ and interaction with the PIDG $g(t,z)$. The amplified optical waves always interact with the PIDG $g(t,z)$ they inscribe, since the Bragg conditions[29-32] $\Delta\omega \equiv \omega^+ - \omega^- = \Omega$, $\beta^+ + \beta^- = q$ are always satisfied. The process of grating inscription is governed by the set of rate equations derived in Appendix B. A self-consistent set of equations enabling simulations of the Brillouin-like amplification in the rare-earth-doped fibers reads as (see, Appendix C for details):

$$\begin{aligned}
&\left(\beta_1 \frac{\partial}{\partial t} + \frac{\partial}{\partial z} \right) e_s^+ = \frac{(1-i\kappa)}{2} \left(\Lambda e_s^+ + g e_s^- \right) + i\kappa W_s e_s^+ \\
&\left(\beta_1 \frac{\partial}{\partial t} - \frac{\partial}{\partial z} \right) e_s^- = \frac{(1-i\kappa)}{2} \left(\Lambda e_s^- + g^* e_s^+ \right) + i\kappa W_s e_s^- \\
&\tau_G \frac{d\Lambda}{dt} = \frac{W_p p_p - \left(p_p + 1 \right) W_s}{\left(p_p + p_s + 1 \right)} - \Lambda \qquad (3) \\
&\tau_G \frac{dg}{dt} = -\left(1 + i\Delta\omega\tau_G \right) g - \frac{\Lambda}{\left(p_p + p_s + 1 \right)} e_s^+ e_s^{-*} \\
&\frac{n_0}{c} \frac{\partial p_p^\pm}{\partial t} \pm \frac{\partial p_p^\pm}{\partial z} = s \left(\Lambda + W_s \right) p_p^\pm - \alpha_p p_p^\pm
\end{aligned}$$

where $\tau_G = T / \left(p_p + p_s + 1 \right)$ is the local population inversion rise time, $e_s = E_S^\pm / \sqrt{P_{S0}}$, $p_p^\pm = P_P^\pm / P_{P0}$, $p_s^\pm = E_S^\pm E_S^{\pm *} / P_{S0}$, $p_{p,s} = p_{p,s}^+ + p_{p,s}^-$, are optical fields and powers normalized to the corresponding saturation powers P_{S0} and P_{p0}; $\Lambda \equiv G - W_s$ is the net gain factor; W_p and W_s are the stimulated transition rates between the ground and excited states for ω_P and signal $\omega^\pm$ frequencies, respectively; T is the rare-earth ion lifetime, $s = P_{s0}\omega_P / P_{p0}\,\omega^\pm$, κ is the ratio between amplitudes of the phase and amplitude gratings (determined by the polarizability difference[27]).

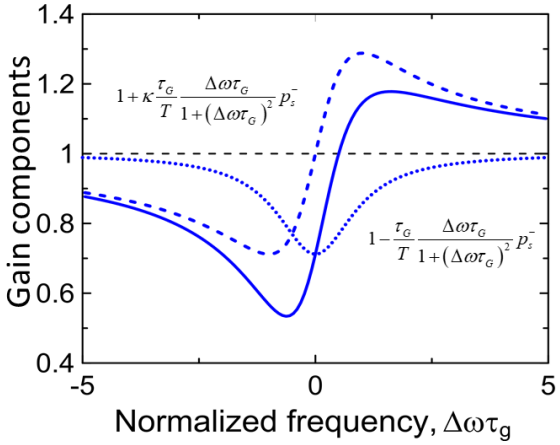

Figure 3. Local gain spectrum for p^+ (blue curve) and its decomposition by terms in brackets of Eq.5.
($p_s^+ \tau_G / T = 0.3$ is taken for calculation).

In Eqs.3, the first two equations describe propagation of two optical monochromatic waves through the fiber. In these two equations the first terms in brackets are responsible for amplification of the signals through the population inversion mechanism. The second terms describe interactions of the signal waves with the backward waves through the dynamical

grating. The latter terms are similar to the corresponding terms in Brillouin equations and are responsible for the Brillouin-like effect. The third equation describes the optical gain factor provided by the population inversion mechanism in the fiber. One can see that the rise time function τ_G determined by the Yb-ion lifetime T and all operating powers sets a pace to all transition processes in the system. Also, the function τ_G characterizes the local lifetime of dynamical grating governed by the fourth equation. One can see that, in contrast to the stationary fiber Bragg grating [33-38], the dynamical grating exists in the fiber only when the fiber is exposed to the interference pattern. Once exposure is terminated (or the interference pattern is shifted), the grating amplitude decays exponentially with the characteristic time τ_G referred to as the local grating lifetime. Specifically, for PIDG, the grating lifetime τ_G decreases with an increase of the operating powers. In this sense, higher operating powers support faster erase of the grating. One can see that the dynamical grating inscribed by the counterpropagating waves of equal frequencies ($\Delta\omega = 0$) is stationary (its position is fixed). Otherwise ($\Delta\omega \neq 0$), the interference pattern moves through the fiber in positive (if $\Delta\omega > 0$) or negative (if $\Delta\omega > 0$) direction with the velocity $V \approx c\Delta\omega/2\tilde{\omega}n$ inscribing the moving gratings. The moving gratings could be thought as a permanent process of the grating re-inscription: each time a new grating is inscribed at a new position, while the previous grating is erased. In these terms, the efficiency of the grating inscription (i.e. the grating amplitude) depends on the grating velocity V in relation to the grating period $\sim \pi c/\tilde{\omega}n$ divided by the grating lifetime τ_G. Inscription is most efficient for the stationary gratings ($V = 0$, $\Delta\omega = 0$) and becomes weak at $\Delta\omega\tau_G \sim \pi$, when the interference pattern is shifted by a half of the grating period for the grating lifetime. The last two equations in Eq.3 are common equations from the two-level laser model[39] describing the dynamics of the pump powers. This dynamics has a minor effect on the Brillouin-like amplification but may complicate its observation. It is for this reason, an Yb-doped double-clad fiber possessing trivial pump dynamics is select here for numerical demonstration of the effect (Table 1).

For steady state power distributions over the fiber Eq.3 is reduced to:

$$\frac{\partial}{\partial z}\ln p_s^{\pm} = \pm\Lambda\left[1-\frac{\tau_G}{T}\frac{1}{1+\left(\Delta\omega\tau_G\right)^2}p_s^{-} \pm \frac{\tau_G}{T}\frac{\kappa\Delta\omega\tau_G}{1+\left(\Delta\omega\tau_G\right)^2}p_s^{-}\right] \tag{4}$$

providing the steady-state net gain Λ and the grating local lifetime τ_G as:

$$\Lambda = \frac{W_p p_p - \left(p_p+1\right)W_s}{\left(p_p+p_s+1\right)}$$

$$\frac{\tau_G}{T} = \frac{1}{\left(p_p+p_s+1\right)}$$

Table 1. Parameters of the Yb-doped fiber amplifier used for calculations

Symbol	Quantity	Value
λ_P	Pump wavelength	975 *nm*
λ_S	Optical signal wavelength	1060 *nm*
$\sigma_{12}^{(p)}$	Effective pump absorption cross sections	$2.69\cdot10^{-24}m^2$
$\sigma_{21}^{(p)}$	Effective pump emission cross sections	$2.97\cdot10^{-24}m^2$
$\sigma_{12}^{(s)}$	Effective signal absorption cross sections	$4.6\cdot10^{-27}m^2$
$\sigma_{21}^{(s)}$	Effective signal emission cross sections	$3.0\cdot10^{-25}cm^2$
N_{Yb}	Concentration of Yb ions in the fiber core	$10.4\cdot10^{19}$
r_P	Radius of the fiber inner cladding	$65\cdot10^{-6}$ *m*
r_S	Radius of the fiber core	$2.5\cdot10^{-6}$ *m*
T	Yb-ion lifetime in the excited state	$0.85\cdot10^{-3}$ *s*
Δp_d	Polarizability difference	$1.2\cdot10^{-32}cm^3$
F_L	Lorentz factor	1.42
κ	Ratio of phase and gain grating amplitudes	2.68

3. SIMULATION RESULTS AND DISCUSSION

In Eq.4 the first term in the brackets is responsible for signal amplification through the population inversion mechanism. The second term describes a decrease of the gain due to the hole burning effect[40]. Its origin is the deconstructive interference of the wave passed through the grating and another wave reflected by the grating. The third term highlights the Brillouin-like effect, i.e., the effect of power transfer from one monochromatic wave to another through the interaction with the dynamical grating these two waves inscribe. Figure 3 shows the total gain spectrum decomposed into these three contributions at a fixed fiber point. The first mechanism does not depend on the frequency difference $\Delta\omega$. It dominates at $\Delta\omega = \infty$ when the contribution of two other mechanisms is negligible. The second mechanism (hole burning) is the most pronounced at $\Delta\omega = 0$ when the recorded dynamic grating is static (its velocity $V = c/2n\ \Delta\omega/\omega \to 0$) and the grating amplitude is maximal. In this case, the amplified wave and the optical wave reflected from the dynamic grating are strictly in antiphase and their coherent annihilation causes a decrease of the net amplification. The effect is symmetrical in respect to $\Delta\omega$ and, therefore, similarly influences both waves. With an increase of $|\Delta\omega| > 0$, the velocity of the moving grating increases and the grating amplitude decreases leading to mitigation of the hole burning effect. The effect described by the third term is caused by a phase part of the population inversion dynamic grating and is proportional to κ. It is asymmetrical in respect to $\Delta\omega$, i.e., the wave possessing higher frequency is always amplified at the expense of the wave possessing lower frequency. Similar to the SBS, the same gain (nonlinear loss) factor is responsible for the gain experienced by one wave and the nonlinear losses experienced by the second wave. Similar to SBS, the gain (nonlinear loss) increment of one wave is proportional to the power of the second wave. The effect is negligible in the limit cases of $\Delta\omega = \infty$ and $\Delta\omega = 0$, and is more pronounced at $\Delta\omega\tau_G \sim 1$. The combined action of all three mechanisms leads to a characteristic gain spectrum exhibiting resonant and anti-resonant peaks. The maximal and minimal gain frequencies are determined by $\Delta\omega_0\tau_G = \left(1+\sqrt{1+\kappa^2}\right)\Big/\kappa$ and $\left(-1+\sqrt{1+\kappa^2}\right)\Big/\kappa$, respectively.

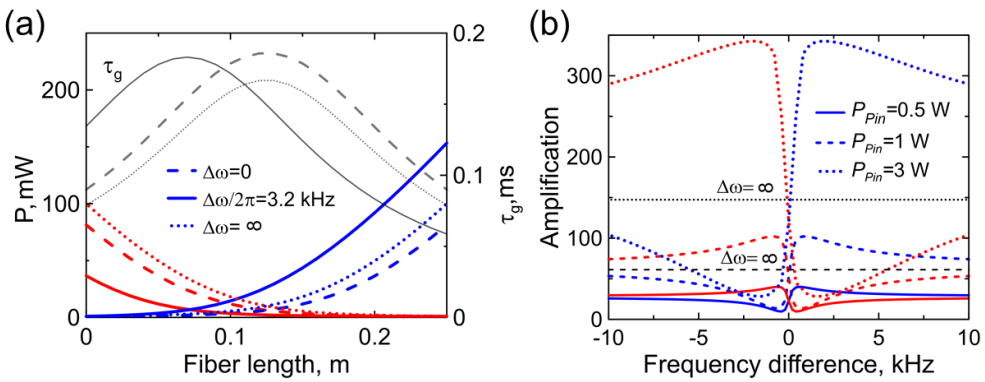

Figure 4. Steady-state solutions of Eq.4 for the 25-cm-length pumped fiber.

(a) Distributions of the optical signal powers and τ_g along the fiber at different $\Delta\omega$ ($P_{Pin} = 1.5W$).

(b) Signal amplification as a function of the frequency difference $\Delta\omega$. The input signal powers are $1mW$.

The steady-state solution described by Eq. 4 (combined with Eq.5 and last two equations in Eqs.3 omitting derivatives in time) highlights the effect of the Brillouin-like amplification. The solution for a 25-cm-length Yb-doped fiber length has been obtained numerically using the Runge-Kutta algorithm. The boundary conditions are $P_S^+(0) = P_{Sin}^+$; $P_S^-(L) = P_{Sin}^-$; $P_P^+(0) = P_P^-(0) = P_{Pin}/2$, where P_{Sin}^+, P_{Sin}^-, P_{Pin} are the signal and input powers. The specific double-clad Yb-doped fiber parameters used in simulations throughout the paper are listed in Table 1. Fig. 4(a) shows typical steady-state power distributions of the interacting waves along the fiber at different values of $\Delta\omega$. The pump power is $P_{Pin} = 1.5W$ and the optical signal inputs are $P_{Sin}^+ = P_{Sin}^- = 1mW$. The curves calculated at $\Delta\omega = \infty$ describe the amplification of optical signals through the population inversion mechanism in the rare-earth optical amplifier. The

counterpropagating optical signals experience amplification independently without mutual interaction. Thanks to symmetry of the setup and two-side pumping both optical signals starting from the same input power acquire the same total amplification equal to $P_S^+(L)/P_{\mathrm{Sin}}^+ = P_S^-(0)/P_{\mathrm{Sin}}^- = 100$. Comparing the curves obtained at $\Delta\omega = 0$ and $\Delta\omega = \infty$ one can see the hole-burning effect. The net amplification achieved at $\Delta\omega = 0$ is ~1.2 times lower (factor A) than that obtained in the case of independent amplification of two waves ($\Delta\omega = \infty$). Both curves exhibit strong symmetry in respect to the midpoint of the fiber and $P_S^+(L)/P_{\mathrm{Sin}}^+ = P_S^-(0)/P_{\mathrm{Sin}}^- = 81.3$. A comparison of the curves obtained at $\Delta\omega = 0$ and $\Delta\omega/2\pi = 3.2kHz$ highlights the Brillouin-like effect providing stronger amplification to the wave possessing higher frequency at expense of the wave possessing lower frequency. One can see that the output power of the signal at higher frequency is 1.53 times higher than its output power without interaction (at $\Delta\omega = \infty$) (factor B) and it is 4.25 times higher than the output power of the signal at lower frequency (factor C). The factors A, B and C introduced here are used as numbers characterizing efficiency of the hole-burning effect (factor A), the Brillouin-like amplification effect (factor B) and symmetry breaking of the amplification line (factor C).

Figure 4(b) shows the net amplification achieved for two counterpropagating optical signal as a function of the frequency difference $\Delta\omega$. One can see that with two-side pumping at $P_{Pin} = 0.5W$ it exhibits an asymmetric profile with the maximum at $0.7kHz$ and minimum at $-0.5kHz$. The resonance peaks are less pronounced than those shown in Fig.3 due to an inhomogeneous broadening associated with nonuniform distribution of the grating relaxation time τ_G over the fiber length shown in Fig.4(a). However, the key features predicted by the third term in Eqs.4 are still pronounced. In particular, with an increase of the pump power from $P_{Pin} = 0.5W$ to $P_{Pin} = 3W$ the maximum peak resonant frequency shifts from $0.7kHz$ to $2kHz$ and the minimum peak resonant frequency shifts from $-0.5kHz$ to $-1.6kHz$. These shifts are accompanied by an increase of the peak amplification $P_S^+(L)/P_{\mathrm{Sin}}^+$ from 41 to 342 and an increase of the factor B and C from 1.45 to 1.7 and from 3.7 to 11.8, respectively, while the factor A remains at the level of 1.22.

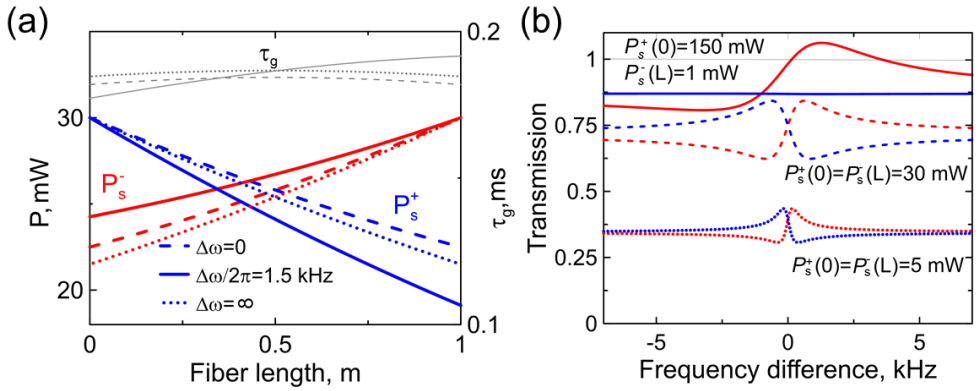

Figure 5. Steady-state solutions of Eq.4 for the 1-m-length unpumped fiber.
Distributions of the optical signal powers and τ_g along the fiber at different $\Delta\omega$, $P_{Sin}^+ = P_{Sin}^- = 30mW$ (a). Signal transmission as a function of the frequency difference $\Delta\omega$ (b).

From Fig.4(b) one can conclude that the power exchange between counterpropagating signals occurs from the wave of lower frequency to the wave of higher frequency. It makes the effect different from Brillouin scattering where the wave at higher frequency commonly donates power to the wave at lower frequency. This difference can be explained in terms of the sign of refractive index modulation induced by the interference pattern $I(t,z)$ produced by a pair of interacting waves. In the case of the Brillouin amplification, the BDG (i.e., the acoustic waves) are produced through the electrostriction effect that increases the fiber glass density and, hence, the refractive index at fiber points exposed to higher light intensity. In contrast, similar exposure in the pumped rare-earth doped fibers reduces the population inversion and, hence, the refractive index. So, for the BDG $\delta n(t,z) \sim I(t,z)$, but for the population inversion gratings in the pumped rare-earth-doped fiber $\delta n(t,z) \sim -I(t,z)$. The power transfer from the wave at higher frequency to the wave at lower frequency is available with unpumped rare-earth-doped fibers. Indeed, $P_{P0}^+ = P_{P0}^- = 0$ for the unpumped

fibers and the function $\Lambda < 0$ in Eqs.4, 5. In Eq.4 the Brillouin-like effect is still described by the third term in brackets, while the second term at $\Lambda < 0$ describes the induced transparency.

The similar steady-state solutions shown in Fig.5 describe the effect of the Brillouin-like amplification in a 1-m-length of unpumped Yb-doped fiber. Fig. 5(a) shows typical steady-state power distributions of the interacting waves along the fiber at different values of $\Delta\omega$. The powers of the input optical signals are $P_{Sin}^{+} = P_{Sin}^{-} = 30mW$. The curves calculated at $\Delta\omega = \infty$ describe the transmission of optical signals through the optical amplifier. The observed power absorption occurs independently for two signals due to interaction with Yb-ions in a ground state. Thanks to symmetry of the setup both optical signals starting from the same input power lose the same power getting the total transition equal to $P_S^{+}(L)/P_{Sin}^{+} = P_S^{-}(0)/P_{Sin}^{-} = 0.72$. Comparing the curves obtained at $\Delta\omega = 0$ and $\Delta\omega = \infty$ one can see the effect of the induced transparency. The net transmission achieved at $\Delta\omega = 0$ is ~1.05 times higher (factor A) than that obtained in the case of independent propagation of two waves ($\Delta\omega = \infty$). Similar to Fig. 4(a), both curves exhibit strong symmetry in respect to the midpoint of the fiber and $P_S^{+}(L)/P_{Sin}^{+} = P_S^{-}(0)/P_{Sin}^{-} = 0.75$. Comparison of the curves obtained at $\Delta\omega = 0$ and $\Delta\omega/2\pi = 1.5kHz$ highlights the Brillouin-like effect providing amplification to the wave at lower frequency at expense of the wave at high frequency. One can see that the output power of the signal at lower frequency is 1.13 times higher than its output power without mutual interaction (at $\Delta\omega = \infty$) (factor B) and it is 1.27 times higher than the output power of the signal at higher frequency (factor C). Here, the factors A, B and C characterize the efficiency of the induced transparency (factor A), the Brillouin-like amplification (factor B) and asymmetry of the transmission spectrum (factor C). One can see that with the simulation parameters used and selected $\Delta\omega/2\pi = 1.5kHz$, the Brillouin-like amplification is rather weak to compensate completely the optical signal losses in the fiber. However, the effect could be enhanced with a proper selection of $\Delta\omega$ and increase of the backward wave power.

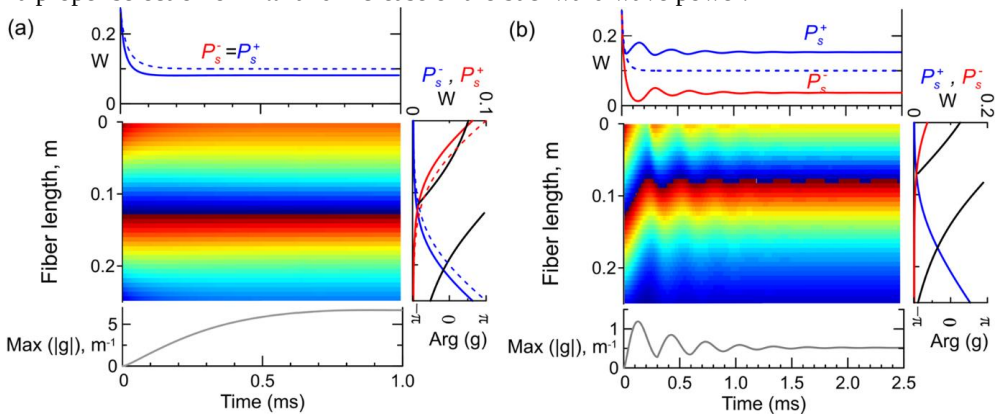

Figure 6. Evolution of the optical signal powers calculated from Eq.1 for the 25-cm-length pumped fiber at $\Delta\omega = 0$ (a) and $\Delta\omega = 3.2\ kHz$ (b). Pump power is ~1.5W, input signal powers are 1mW.

Figure 5(b) shows the net transmission achieved for two counterpropagating optical signals as a function of the frequency difference $\Delta\omega$. One can see that the transmission of one wave depends on the frequency difference $\Delta\omega$ and power of the second wave. With an increase of the second wave power from 5 to 150mW the resonant frequency difference shifts from $-0.13Hz$ to $-1.3kHz$ and the peak transmittance for the primary wave increases from 44% to 106%. Thus, the increase of the wave power of lower frequency occurs at expense of the wave power of higher frequency making the effect even more similar to stimulated Brillouin scattering. It is explained by the fact that in the unpumped ($\Lambda < 0$) rare-earth doped fibers the interference pattern $I(t,z)$ produced by a pair of interacting waves increases the population inversion and, hence, the refractive index in fiber points exposed to higher intensity. So, for the population inversion grating in this case $\delta n(t,z) \sim I(t,z)$, like in the traditional SBS.

Finally, we have performed numerical simulations of the temporal-spatial differential Eq.3 to explore the formation of the dynamical grating in the pumped rare-earth-doped fiber and to analyze evolution of the optical signals to the steady-state solution (Eq.4). The fourth-order Runge–Kutta algorithm has been adapted for this purpose. The used initial and boundary conditions are $P_P^{+}(0,z) = P_P^{-}(0,z) = P_{Pin}/2$; $P_S^{+}(0,z) = P_S^{-}(0,z) = 0$; $P_P^{+}(t,0) = P_P^{-}(t,L) = P_{Pin}/2$,

$P_S^+(t,0) = P_{\text{Sin}}^+$; $P_S^+(t,L) = P_{\text{Sin}}^-$. The phases of the input optical signals are constants. The results of this simulations at $\Delta\omega = 0$ and $\Delta\omega = 3.2\ kHz$ are compared in Fig.6 (a) and (b), respectively. We again consider a 25-cm-length Yb-doped fiber pumped by $P_{Pin} = \sim 1.5W$ from two sides. In both cases, two monochromatic signals with the input powers of ~1mW are introduced into the fiber from the opposite fiber ends. At the moment of time $t = 0$, the forward front of the optical signal wave gets the fiber output possessing the peak output power of ~270 mW determined by the amplifier transient characteristics. The amplitude of the dynamical grating is close to zero, since the process of the grating inscription is not started yet. Further evolution of the interacting fields depends on the frequency difference $\Delta\omega$. At $\Delta\omega = 0$ an increase of the grating amplitude caused by the interference pattern leads to suppression of net amplification in the fiber due to hole-burning effect. The output powers of both optical signals decrease down to ~81mW that is by ~ 15mW lower than the steady-state output power at $\Delta\omega = \infty$ (see, dashed line for comparison). The typical time of the grating evolution to the steady-state is ~0.1ms. One can see that the phase of the grating complex amplitude $\arg g(t,z)$ monotonically changes over the fiber length due to additional phase shift acquired (through the RIC effect) by the interacting signals during amplification. Importantly, the profile $\arg g(t,z)$ does not change in time at $\Delta\omega = 0$. At $\Delta\omega = 3.2kHz$ the behavior of the interacting fields is qualitatively different. The dynamical grating is inscribed by the moving interference pattern with the velocity estimated as $V \approx c\Delta\omega/2\tilde{\omega}n \sim 1.13cm/s$. In comparison with Fig.6 (a), this feature is reflected in a lower steady-state grating amplitude and longer time of transition to steady-state with recognized re-oscillations shown in the graph of $\max|g(z)|(t)$. The profile $\arg g(t,z)$ still possesses the monotonic change with the fiber length, but also performs weak relaxing perturbations in time of the grating velocity. The dynamical grating moving along the fiber in the positive direction breaks the symmetry and provides preferable amplification of the wave of higher frequency. The steady-state output powers are ~36mW and ~154mW for the lower and higher frequency waves, respectively. The steady-state distribution $\arg g(z)$ is steeper than the similar distribution at $\Delta\omega = 0$. The steady-state solution is well described by Eq. 4.

4. CONCLUSION

In conclusion, we have described the interaction of two counterpropagating monochromatic waves in a doped optical fiber amplifier demonstrating a strong power transfer from one wave to another. The phenomenon is explained as a reverse effect of the PIDG inscribed by the counterpropagating optical waves in the active fiber. A self-consistent set of equations enabling description of a number of effects governed by the population inversion mechanism, like an optical gain, hole-burning, population inversion grating, laser frequency self-scanning, and so on, is derived and applied to demonstrate the Brillouin-like amplification in rare-earth doped fibers. We have shown that the propagation of the monochromatic wave through the active fiber could provide the wave propagating in the backward direction with an additional gain shifted in frequency by some value in the kHz range. The effect is demonstrated for the configuration of a bidirectional rare-earth-doped optical fiber amplifier. We have shown that in contrast to SBS, the power transfer in the rare-earth-doped fibers could occur either to the wave with higher (anti-Stokes) or lower (Stokes) frequency. Anti-Stokes wave amplification is dominating in the pumped fibers, while amplification of the Stokes wave can occur in fibers without pumping. We believe that the reported Brillouin-like effect could be employed in many new photonics devices expanding the range of the traditional Brillouin applications (fiber lasers, microwave photonics, distributed sensors, spectrometry) to the sub-kHz frequency domain. Similar to SBS, the reported narrowband amplitude response is accompanied by a strong dispersive response, able to tailor the phase or group delay of a backward optical signal. In light of these effects, the Brillouin-like amplification could enrich the advanced Brillouin applications such as slow light[41-44], stored light[45-48], narrowband RF photonic filters[49-51], optical processing[52-54], distributed sensing[55-60], narrowband spectrometers[61, 62], optical amplifiers[63], narrow linewidth, spectrally pure RF sources[64, 65] among others. The PIDG analog of the forward Brillouin scattering in optical fibers[66-71] could be of particular interest for further studies due to its enormous potential for practical applications in soliton fiber lasers as the method enabling the stabilization of harmonically mode-locked laser operation and super-mode noise reduction[72-77]. New mechanisms are important as well for designers of the Brillouin and random fiber lasers[78-93] demanded in many applications in microwave photonics, data centers and atomic clocks. Translating the fiber system design to integrated photonics could dramatically reduce the footprint for many these applications[94-97].

ACKNOWLEDGEMENTS

The work was supported by the RSF (#23-79-30017). A.F. is supported by the European Union's Horizon 2020 research and innovation programme (H2020-MSCA–IF–2020, #101028712).

REFERENCES

[1] Eichler, H. J., Günter, P., and Pohl, D. W., [Laser-induced dynamic gratings], Springer (2013).
[2] Song, K. Y., and Yoon, H. J., "Observation of narrowband intrinsic spectra of brillouin dynamic gratings," Opt Lett 35, 2958-2960 (2010).
[3] Santagiustina, M., Chin, S., Primerov, N., Ursini, L., and Thévenaz, L., "All-optical signal processing using dynamic brillouin gratings," Scientific reports 3, 1594 (2013).
[4] Wolff, C., Steel, M. J., Eggleton, B. J., and Poulton, C. G., "Stimulated brillouin scattering in integrated photonic waveguides: Forces, scattering mechanisms, and coupled-mode analysis," Physical Review A 92 (2015).
[5] Dong, Y., Zhang, H., Zhou, D., Bao, X., & Chen, L. , "Characterization of brillouin gratings in optical fibers and their applications," in Fiber optic sensors (2012).
[6] He, Z., and Hotate, K., "Dynamic gratings in optical fibers: Synthesis and sensing applications," Photonic Sensors 2, 60-64 (2012).
[7] Lopez-Mercado, C. A., Korobko, D. A., Zolotovskii, I. O., and Fotiadi, A. A., "Application of dual-frequency self-injection locked dfb laser for brillouin optical time domain analysis," Sensors 21, 6859 (2021).
[8] Stepanov, S., "Dynamic population gratings in rare-earth-doped optical fibres," Journal of Physics D: Applied Physics 41, 224002 (2008).
[9] Melle, S., Calderón, O. G., Zhuo, Z. C., Antón, M. A., and Carreño, F., "Dynamic population gratings in highly doped erbium fibers," Journal of the Optical Society of America B 28, 1631-1637 (2011).
[10] Lobach, I. A., Kablukov, S. I., Podivilov, E. V., Fotiadi, A. A., and Babin, S. A., "Fourier synthesis with single-mode pulses from a multimode laser," Optics Letters 40, 3671 (2015).
[11] Lobach, I. A., Drobyshev, R. V., Fotiadi, A. A., Podivilov, E. V., Kablukov, S. I., and Babin, S. A., "Open-cavity fiber laser with distributed feedback based on externally or self-induced dynamic gratings," Optics Letters 42, 4207 (2017).
[12] Budarnykh, A., Lobach, I., and Kablukov, S., "Self-sweeping tm-doped fiber laser with wavelength stopping," Laser Physics Letters 16, 025108 (2019).
[13] Rivera, J. L., Sánchez, M. P., Miridonov, A., and Stepanov, S., "Adaptive sagnac interferometer with dynamic population grating in saturable rare-earth-doped fiber," Opt. Express 21, 4280-4290 (2013).
[14] Stepanov, S., and Cota, F. P., "Transient two-wave mixing in a linear configuration of an adaptive interferometer based on er-doped fiber with saturable absorption," Optics Letters 32, 2532-2534 (2007).
[15] Popov, S. M., Butov, O. V., Chamorovski, Y. K., Isaev, V. A., Mégret, P., Korobko, D. A., Zolotovskii, I. O., and Fotiadi, A. A., "Narrow linewidth short cavity brillouin random laser based on bragg grating array fiber and dynamical population inversion gratings," Results in Physics 9, 806-808 (2018).
[16] Popov, S. M., Butov, O. V., Bazakutsa, A. P., Vyatkin, M. Y., Chamorovskii, Y. K., and Fotiadi, A. A., "Random lasing in a short er-doped artificial rayleigh fiber," Results in Physics 16, 102868 (2020).
[17] Aguilar, E., Stepanov, S., and Hernandez, E., "High-resolution adaptive interferometer with dynamic population grating recorded at 1064 nm in ytterbium-doped fiber," Applied Optics 59, 6131-6137 (2020).
[18] Bliokh, Y., Chaikina, E. I., Vatnik, I. D., and Churkin, D. V., "Temporal variation of the spectrum of a continuously pumped random fiber laser: Phenomenological model," Journal of the Optical Society of America B 36, 408-414 (2019).
[19] Agrawal, G., [Nonlinear fiber optics], © Academic Press 2001 (2001).
[20] Eggleton, B. J., Poulton, C. G., and Pant, R., "Inducing and harnessing stimulated brillouin scattering in photonic integrated circuits," Adv. Opt. Photon. 5, 536-587 (2013).
[21] Fotiadi, A. A., Korobko, D. A., Zolotovskii, I. O., and Taylor, J. R., "Brillouin-like amplification in rare-earth-doped optical fibers," Opt. Express 29, 40345-40359 (2021).
[22] Boyd, R. W., Rzązewski, K., and Narum, P., "Noise initiation of stimulated brillouin scattering," Physical Review A 42, 5514-5521 (1990).
[23] Gaeta, A. L., and Boyd, R. W., "Stochastic dynamics of stimulated brillouin scattering in an optical fiber," Physical Review A 44, 3205 (1991).

[24] Boyd, R. W., [Nonlinear optics], Academic press (2020).
[25] Smith, S. P., Zarinetchi, F., and Ezekiel, S., "Narrow-linewidth stimulated brillouin fiber laser and applications," Optics Letters 16, 393-395 (1991).
[26] Paschotta, R., Nilsson, J., Tropper, A. C., and Hanna, D. C., "Ytterbium-doped fiber amplifiers," IEEE Journal of Quantum Electronics 33, 1049-1056 (1997).
[27] Fotiadi, A. A., Antipov, O. L., and Mégret, P., "Dynamics of pump-induced refractive index changes in single-mode yb-doped optical fibers," Opt. Express 16, 12658 (2008).
[28] Pask, H., Carman, R. J., Hanna, D. C., Tropper, A. C., Mackechnie, C. J., Barber, P. R., and Dawes, J. M., "Ytterbium-doped silica fiber lasers: Versatile sources for the 1-1.2/spl mu/m region," IEEE Journal of Selected Topics in Quantum Electronics 1, 2-13 (1995).
[29] Shen, Y. R., and Bloembergen, N., "Theory of stimulated brillouin and raman scattering," Physical Review 137, A1787 (1965).
[30] Starunov, V. S., and Fabelinskii, I. L., "Stimulated mandel'shtam–brillouin scattering and stimulated entropy (temperature) scattering of light," Uspekhi Fizicheskih Nauk 98, 441-491 (1969).
[31] Stolen, R., "Polarization effects in fiber raman and brillouin lasers," IEEE Journal of Quantum Electronics 15, 1157-1160 (1979).
[32] Tang, C. L., "Saturation and spectral characteristics of the stokes emission in the stimulated brillouin process," Journal of Applied Physics 37, 2945-2955 (1966).
[33] Mescia, L., "Design of long-period gratings in cladding-pumped microstructured optical fiber," JOSA B 25, 1833-1839 (2008).
[34] Prudenzano, F., Mescia, L., Palmisano, T., Surico, M., De Sario, M., and Righini, G. C., "Optimization of pump absorption in mof lasers via multi-long-period gratings: Design strategies," Appl Opt 51, 1420-1430 (2012).
[35] Sabatier, C., Ladaci, A., Girard, S., Mescia, L., Robin, T., Cadier, B., Boukenter, A., Ouerdane, Y., and Marin, E., "Influence of the core dopants on the brillouin signature of specialty optical fibers," (2017).
[36] Girard, S., Morana, A., Ladaci, A., Robin, T., Mescia, L., Bonnefois, J.-J., Boutillier, M., Mekki, J., Paveau, A., and Cadier, B., "Recent advances in radiation-hardened fiber-based technologies for space applications," Journal of Optics 20, 093001 (2018).
[37] Fotiadi, A. A., Brambilla, G., Ernst, T., Slattery, S. A., and Nikogosyan, D. N., "Tpa-induced long-period gratings in a photonic crystal fiber: Inscription and temperature sensing properties," Journal of the Optical Society of America B: Optical Physics 24, 1475-1481 (2007).
[38] Caucheteur, C., Fotiadi, A., Megret, P., Slattery, S. A., and Nikogosyan, D. N., "Polarization properties of long-period gratings prepared by high-intensity femtosecond 352-nm pulses," IEEE Photonics Technology Letters 17, 2346-2348 (2005).
[39] Aubry, M., Mescia, L., Morana, A., Robin, T., Laurent, A., Mekki, J., Marin, E., Ouerdane, Y., Girard, S., and Boukenter, A., "Temperature influence on the radiation responses of erbium-doped fiber amplifiers," physica status solidi (a), 2100002 (2021).
[40] Paschotta, R., Nilsson, J., Reekie, L., Trooper, A. C., and Hanna, D. C., "Single-frequency ytterbium-doped fiber laser stabilized by spatial hole burning," Optics Letters 22, 40-42 (1997).
[41] Thévenaz, L., "Slow and fast light in optical fibres," Nature photonics 2, 474-481 (2008).
[42] Sharma, D. K., and Tripathi, S. M., "Optical performance of tellurite glass microstructured optical fiber for slow-light generation assisted by stimulated brillouin scattering," Optical Materials 94, 196-205 (2019).
[43] Zadok, A., Chin, S., Thévenaz, L., Zilka, E., Eyal, A., and Tur, M., "Polarization-induced distortion in stimulated brillouin scattering slow-light systems," Optics letters 34, 2530-2532 (2009).
[44] Kim, J., Kuzyk, M. C., Han, K., Wang, H., and Bahl, G., "Non-reciprocal brillouin scattering induced transparency," Nature Physics 11, 275-280 (2015).
[45] Merklein, M., Stiller, B., and Eggleton, B. J., "Brillouin-based light storage and delay techniques," Journal of Optics 20, 083003 (2018).
[46] Kalosha, V., Li, W., Wang, F., Chen, L., and Bao, X., "Frequency-shifted light storage via stimulated brillouin scattering in optical fibers," Optics letters 33, 2848-2850 (2008).
[47] Pang, M., He, W., Jiang, X., and Russell, P. S. J., "All-optical bit storage in a fibre laser by optomechanically bound states of solitons," Nature Photonics 10, 454 (2016).
[48] Merklein, M., Stiller, B., Vu, K., Madden, S. J., and Eggleton, B. J., "A chip-integrated coherent photonic-phononic memory," Nature Communications 8, 574 (2017).

[49] Marpaung, D., Morrison, B., Pagani, M., Pant, R., Choi, D.-Y., Luther-Davies, B., Madden, S. J., and Eggleton, B. J., "Low-power, chip-based stimulated brillouin scattering microwave photonic filter with ultrahigh selectivity," Optica 2, 76-83 (2015).
[50] Pang, Y., Xu, Y., Zhao, X., Qin, Z., and Liu, Z., "Low-noise brillouin random fiber laser with auto-tracking dynamic fiber grating based on a saturable absorption ring," Infrared Physics & Technology, 104088 (2022).
[51] Gertler, S., Kittlaus, E. A., Otterstrom, N. T., and Rakich, P. T., "Tunable microwave-photonic filtering with high out-of-band rejection in silicon," APL Photonics 5, 096103 (2020).
[52] Choudhary, A., Morrison, B., Aryanfar, I., Shahnia, S., Pagani, M., Liu, Y., Vu, K., Madden, S., Marpaung, D., and Eggleton, B. J., "Advanced integrated microwave signal processing with giant on-chip brillouin gain," Journal of Lightwave Technology 35, 846-854 (2017).
[53] Liu, Y., Choudhary, A., Marpaung, D., and Eggleton, B. J., "Chip-based brillouin processing for phase control of rf signals," IEEE Journal of Quantum Electronics 54, 1-13 (2018).
[54] Merklein, M., Casas-Bedoya, A., Marpaung, D., Büttner, T. F. S., Pagani, M., Morrison, B., Kabakova, I. V., and Eggleton, B. J., "Stimulated brillouin scattering in photonic integrated circuits: Novel applications and devices," IEEE Journal of Selected Topics in Quantum Electronics 22, 336-346 (2016).
[55] Bergman, A., Langer, T., and Tur, M., "Coding-enhanced ultrafast and distributed brillouin dynamic gratings sensing using coherent detection," Journal of Lightwave Technology 34, 5593-5600 (2016).
[56] Zhang, H., Zhou, D., Wang, B., Pang, C., Xu, P., Jiang, T., Ba, D., Li, H., and Dong, Y., "Recent progress in fast distributed brillouin optical fiber sensing," Applied Sciences 8 (2018).
[57] Bueno Escobedo, J. L., Jason, J., López-Mercado, C. A., Spirin, V. V., Wuilpart, M., Mégret, P., Korobko, D. A., Zolotovskiy, I. O., and Fotiadi, A. A., "Distributed measurements of vibration frequency using phase-otdr with a dfb laser self-stabilized through pm fiber ring cavity," Results in Physics 12, 1840-1842 (2019).
[58] Lopez-Mercado, C. A., Korobko, D. A., Zolotovskii, I. O., and Fotiadi, A. A., "Application of dual-frequency self-injection locked dfb laser for brillouin optical time domain analysis," Sensors (Basel) 21 (2021).
[59] Gorshkov, B. G., Yüksel, K., Fotiadi, A. A., Wuilpart, M., Korobko, D. A., Zhirnov, A. A., Stepanov, K. V., Turov, A. T., Konstantinov, Y. A., and Lobach, I. A., "Scientific applications of distributed acoustic sensing: State-of-the-art review and perspective," Sensors 22, 1033 (2022).
[60] Bueno Escobedo, J. L., Spirin, V. V., López-Mercado, C. A., Márquez Lucero, A., Mégret, P., Zolotovskii, I. O., and Fotiadi, A. A., "Self-injection locking of the dfb laser through an external ring fiber cavity: Application for phase sensitive otdr acoustic sensor," Results in Physics 7, 641-643 (2017).
[61] Dong, Y., Jiang, T., Teng, L., Zhang, H., Chen, L., Bao, X., and Lu, Z., "Sub-mhz ultrahigh-resolution optical spectrometry based on brillouin dynamic gratings," Optics letters 39, 2967-2970 (2014).
[62] Faustov, A. V., Gusarov, A. V., Mégret, P., Wuilpart, M., Zhukov, A. V., Novikov, S. G., Svetukhin, V. V., and Fotiadi, A. A., "The use of optical frequency-domain reflectometry in remote distributed measurements of the γ-radiation dose," Technical Physics Letters 41, 414-417 (2015).
[63] Raupach, S. M., Koczwara, A., and Grosche, G., "Brillouin amplification supports 1×10^{-20} uncertainty in optical frequency transfer over 1400 km of underground fiber," Physical Review A 92, 021801 (2015).
[64] McKay, L., Merklen, M., Liu, Y., Cramer, A., Maksymow, J., Chilton, A., Yan, K., Choi, D.-Y., Madden, S. J., DeSalvo, R., and Eggleton, B. J., "Integrated microwave photonic true-time delay with interferometric delay enhancement based on brillouin scattering and microring resonators," Opt. Express 28, 36020-36032 (2020).
[65] Jia, Q., Zhang, P., Wang, T., Li, X., and Bo, B., "40 ghz narrow linewidth frequency-switched microwave signal generation based on a single-longitudinal-mode double-brillouin-frequency spaced brillouin fiber laser," Applied Optics 56, 5323-5328 (2017).
[66] Shelby, R. M., Levenson, M. D., and Bayer, P. W., "Guided acoustic-wave brillouin scattering," Physical Review B 31, 5244-5252 (1985).
[67] Shelby, R., Levenson, M., and Bayer, P., "Resolved forward brillouin scattering in optical fibers," Physical review letters 54, 939 (1985).
[68] Liu, Y., Ning, Y., Gu, Y., Chen, P., Jiang, K., Wang, L., You, Y., He, W., and Chou, X., "Ultra-narrow linewidth dual-cavity opto-mechanical microwave oscillator based on radial guided acoustic modes of single-mode fiber," Applied Physics Letters 122, 041107 (2023).
[69] Sánchez, L. A., Díez, A., Cruz, J. L., and Andrés, M. V., "High accuracy measurement of poisson's ratio of optical fibers and its temperature dependence using forward-stimulated brillouin scattering," Opt. Express 30, 42-52 (2022).
[70] Sánchez, L. A., Díez, A., Cruz, J. L., and Andrés, M. V., "Recent advances in forward brillouin scattering: Sensor applications," in Sensors(2023).

[71] Sánchez, L. A., Díez, A., Cruz, J. L., and Andrés, M. V., "Efficient interrogation method of forward brillouin scattering in optical fibers using a narrow bandwidth long-period grating," Optics Letters 45, 5331-5334 (2020).
[72] Ribenek, V. A., Stoliarov, D. A., Korobko, D. A., and Fotiadi, A. A., "Pulse repetition rate tuning of a harmonically mode-locked ring fiber laser using resonant optical injection," Optics Letters 46, 5687-5690 (2021).
[73] Ribenek, V. A., Stoliarov, D. A., Korobko, D. A., and Fotiadi, A. A., "Mitigation of the supermode noise in a harmonically mode-locked ring fiber laser using optical injection," Optics Letters 46, 5747-5750 (2021).
[74] Ribenek, V. A., Korobko, D. A., Fotiadi, A. A., and Taylor, J. R., "Supermode noise mitigation and repetition rate control in a harmonic mode-locked fiber laser implemented through the pulse train interaction with co-lased cw radiation," Optics Letters 47, 5236-5239 (2022).
[75] Korobko, D. A., Ribenek, V. A., Itrin, P. A., and Fotiadi, A. A., "Birth and annihilation of solitons in harmonically mode-locked fiber laser cavity through continuous wave injection," Optical Fiber Technology 75, 103216 (2023).
[76] Korobko, D. A., Ribenek, V. A., Itrin, P. A., Stoliarov, D. A., and Fotiadi, A. A., "Polarization maintaining harmonically mode-locked fiber laser with suppressed supermode noise due to continuous wave injection," Optics & Laser Technology 162, 109284 (2023).
[77] Kbashi, H. J., Sergeyev, S. V., Al-Araimi, M., Rozhin, A., Korobko, D., and Fotiadi, A., "High-frequency vector harmonic mode locking driven by acoustic resonances," Optics Letters 44, 5112-5115 (2019).
[78] Bueno Escobedo, J. L., Spirin, V. V., López-Mercado, C. A., Mégret, P., Zolotovskii, I. O., and Fotiadi, A. A., "Self-injection locking of the dfb laser through an external ring fiber cavity: Polarization behavior," Results in Physics 6, 59-60 (2016).
[79] Korobko, D. A., Zolotovskii, I. O., Panajotov, K., Spirin, V. V., and Fotiadi, A. A., "Self-injection-locking linewidth narrowing in a semiconductor laser coupled to an external fiber-optic ring resonator," Optics Communications 405, 253-258 (2017).
[80] Spirin, V. V., Bueno Escobedo, J. L., Korobko, D. A., Mégret, P., and Fotiadi, A. A., "Stabilizing dfb laser injection-locked to an external fiber-optic ring resonator," Opt. Express 28, 478-484 (2020).
[81] Korobko, D., Zolotovskii, I., Svetukhin, V., Zhukov, A., Fomin, A., Borisova, C., and Fotiadi, A., "Detuning effects in brillouin ring microresonator laser," Opt. Express 28, 4962-4972 (2020).
[82] Spirin, V. V., Bueno Escobedo, J. L., Korobko, D. A., Mégret, P., and Fotiadi, A. A., "Dual-frequency laser comprising a single fiber ring cavity for self-injection locking of dfb laser diode and brillouin lasing," Opt. Express 28, 37322-37333 (2020).
[83] Spirin, V. V., Bueno Escobedo, J. L., Miridonov, S. V., Maya Sánchez, M. C., López-Mercado, C. A., Korobko, D. A., Zolotovskii, I. O., and Fotiadi, A. A., "Sub-kilohertz brillouin fiber laser with stabilized self-injection locked dfb pump laser," Optics & Laser Technology 141, 107156 (2021).
[84] Grukh, D. A., Kurkov, A. S., Razdobreev, I. M., and Fotiadi, A. A., "Self-q-switched ytterbium-doped cladding-pumped fibre laser," Quantum electronics 32, 1017 (2002).
[85] Gomes, A. S. L., Moura, A. L., de Araújo, C. B., and Raposo, E. P., "Recent advances and applications of random lasers and random fiber lasers," Progress in Quantum Electronics 78, 100343 (2021).
[86] Zhou, Z., Chen, L., and Bao, X., "High efficiency brillouin random fiber laser with replica symmetry breaking enabled by random fiber grating," Opt. Express 29, 6532-6541 (2021).
[87] Arshad, M. A., Hartung, A., Pratiwi, A. C., and Jäger, M., "Observation of direction instability in a fiber ring laser," Scientific Reports 11, 4436 (2021).
[88] Tehranchi, A., Iezzi, V. L., and Kashyap, R., "Power fluctuations and random lasing in multiwavelength brillouin erbium-doped fiber lasers," Journal of Lightwave Technology 37, 4439-4444 (2019).
[89] Song, Y., Li, S., Zhang, J., Zhang, M., Qiao, L., and Wang, T., "The modeling of random brillouin dynamic grating," Optical Fiber Technology 53, 102034 (2019).
[90] Deng, J., Han, M., Xu, Z., Du, Y., and Shu, X., "Stable and low-threshold random fiber laser via anderson localization," Opt Express 27, 12987-12997 (2019).
[91] Margulis, W., Das, A., von der Weid, J. P., and Gomes, A. S. L., "Hybrid electronically addressable random fiber laser," Opt. Express 28, 23388-23396 (2020).
[92] Kashirina, E. K., Lobach, I. A., and Kablukov, S. I., "Dual-longitudinal-mode cw self-sweeping operation in er-doped fiber laser," Opt Lett 45, 6659-6662 (2020).
[93] Drobyshev, R. V., Poddubrovskii, N. R., Lobach, I. A., and Kablukov, S. I., "High-resolution spectral analysis of long single-frequency pulses generated by a self-sweeping yb-doped fiber laser," Laser Physics Letters 18, 085102 (2021).

[94] Korobko, D. A., Zolotovskii, I. O., Svetukhin, V. V., Zhukov, A. V., Fomin, A. N., Borisova, C. V., and Fotiadi, A. A., "Detuning effects in brillouin ring microresonator laser," Opt Express 28, 4962-4972 (2020).
[95] Phan Huy, K., Nguyen, A. T., Brainis, E., Haelterman, M., Emplit, P., Corbari, C., Canagasabey, A., Kazansky, P. G., Deparis, O., Fotiadi, A. A., Mégret, P., and Massar, S., "Photon pair source based on parametric fluorescence in periodically poled twin-hole silica fiber," Opt. Express 15, 4419 (2007).
[96] Korobko, D. A., Fotiadi, A. A., and Zolotovskii, I. O., "Mode-locking evolution in ring fiber lasers with tunable repetition rate," Opt. Express 25, 21180 (2017).
[97] Preda, C. E., Fotiadi, A. A., and Megret, P., "Numerical approximation for brillouin fiber ring resonator," Opt Express 20, 5783-5788 (2012).